2020

HIGH-PERFORMANCE ZERO LIQUID DISCHARGE (ZLD) TREATMENT OF HIGH-SALINITY BRINES USING A MULTIPLE-EFFECT ABSORPTION DISTILLATION CONCEPT

Sunil Pinnu
Michigan Technological University, spinnu@mtu.edu

HIGH-PERFORMANCE ZERO LIQUID DISCHARGE (ZLD) TREATMENT OF HIGH-SALINITY BRINES USING A MULTIPLE-EFFECT ABSORPTION DISTILLATION CONCEPT

By

Sunilkumar Pinnu

A THESIS

Submitted in partial fulfillment of the requirements for the degree of

MASTER OF SCIENCE

In Mechanical Engineering

MICHIGAN TECHNOLOGICAL UNIVERSITY

2020

This thesis has been approved in partial fulfillment of the requirements for the Degree of MASTER OF SCIENCE in Mechanical Engineering.

Department of Mechanical Engineering-Engineering Mechanics

Thesis Advisor: *Dr. Sajjad Bigham*

Committee Member: *Dr. Fernando Ponta*

Committee Member: *Dr. Kazuya Tajiri*

Department Chair: *Dr. William W. Predebon*

Table of Contents

List of figures

List of tables

Preface

Introduction section consists of images from previously published materials. The images have been included to better understand the thermal and hybrid Zero Liquid Discharge (ZLD) desalination processes and involved processes. The images are copyright of respective authors and none of these have been reproduced in this thesis by any means. Appropriate citing has been included to credit the original papers and authors and official permission has been taken, for each image, for reuse in this thesis.

Acknowledgements

First and foremost, I would like to thank the Almighty God for giving me the strength, patience and knowledge that enabled me to efficiently and effectively finish this thesis.

The entirety of this thesis has been carried out in Energy-X (Energy eXploration Laboratory) of Michigan Technological University during the years 2018-2020, under the guidance of Assistant Professor and Director of Energy eXploration Laboratory, Dr. Sajjad Bigham.

My heartiest thanks are due to my advisor, Dr. Sajjad Bigham, for giving me the opportunity to work on this project and for the constant encouragement, support and guidance provided throughout this thesis.

I would also like to take the opportunity to thank my parents, family and friends for their constant emotional support and encouragement.

Definitions

The following are the list of definitions used in this document along with the units.

D = Mass flowrate of distillate (kg/s)

F = Mass flowrate of feed (kg/s)

B = Mass flowrate of brine (kg/s)

$\dot{m}$ = Mass flowrate (kg/s)

h = enthalpy (J/kg)

X = salinity (g/kg)

x = concentration of LiBr solution

$\dot{Q}$ = Heat transfer rate (kW)

U = Heat transfer coefficient (kW/m^2-K)

A = Heat transfer area (m^2)

T = Temperature (K)

$\dot{w}$ = pumping work (kW)

$C_{p,water}$ = Specific heat of water (kJ/kg-K)

Φ = Mass fraction

P = Pressure (kPa)

v = Specific volume (m^3/kg)

List of abbreviations

ZLD	Zero Liquid Discharge
MED	Multi Effect Desalination
MVC	Mechanical Vapor Compression
LiBr	Lithium Bromide
FCHX	Forced Circulation Heat Exchanger
DU	Desorption Unit
RO	Reverse Osmosis
ED	Electrodialysis
UF	Ultra Filtration
NF	Nano Filtration
MD	Membrane Distillation
MCr	Membrane Crystallization

Abstract

State-of-the-art zero liquid discharge (ZLD) technologies are currently bound with either intensive use of high-grade electrical energy such as mechanical vacuum vapor compressors utilized in brine crystallizers or high capital cost with environmental concerns such as evaporation ponds. The present study aims to address these issues by an innovative desiccant-based ZLD system in which a multiple-effect distillation (MED) unit is uniquely embedded at the heart of an absorption-desorption system. Here, the MED and absorption systems are inherently coupled enabling both heat and mass transfer processes between a high-salinity water and a desiccant solution. The proposed technology employs an absorption-based thermally-driven vapor compressor concept to pressurize the vaporized brine of the ZLD unit from a low-pressure absorber to a high-pressure desorber. The vacuum environment required for the ZLD treatment is established by strong hygroscopic properties of an aqueous lithium bromide (LiBr) salt. This eliminates the need for energy-intensive electrically-driven mechanical vapor compressors currently employed in advanced brine crystallizers. Comprehensive thermodynamic modeling has been performed to evaluate energy efficiency and size of the system. Insights gained from the present study have a high potential to truly transform thermal desalination and, in particular, ZLD treatment industries.

1 Introduction

Freshwater scarcity due to population growth, pollution of water bodies, industrialization, and climate changes has imposed a major threat to future prospect of world economy, environmental sustainability, and human life quality [1–7]. Recycling and reuse of sea/brackish water through desalination has the ability to be considered as a potential solution for increasing global fresh water demands [8–12]. Existing conventional desalination technologies are highly energy intensive to purify saline water with high total dissolved solids (TDS) concentration values (TDS>100,000 ppm), and often unable to economically achieve ZLD operation desired in many industrial applications with high brine disposal costs [13–15]. Current ZLD technologies operate on the principle of evaporation process driven by energy-intensive mechanical vapor compression (MVC) [16–19]. The present study overcomes the drawback of high energy consumption of conventional ZLD systems by replacing the MVC driven evaporation process by an energy efficient thermally driven vapor compression evaporation process.

1.1 Motivation

Securing availability of clean and fresh water is a present challenge faced by many nations [20–25]. Over the past few decades, global fresh water demands have increased due to climate change, depletion of fresh water resources, pollution of fresh water bodies, industrialization, and increasing living standards among others [26–31]. Two-thirds of the world population (i.e., approximate 4 billion people) live in areas with severe water scarcity at least one month in a year with half a billion people facing water scarcity all year round

[32]. United Nations organization estimates that nearly 1800 million people will be under severe water scarcity by 2025 [33]. Increasing water pollution due to industrial pollution also becomes a cause of fresh water scarcity [34]. Industries such as chemical, pharmaceutical, textile, oil and gas eject huge amounts of liquid waste to surrounding water bodies causing massive water pollution both in developing and developed countries [35–37]. In addition, water pollution could immensely affects quality of human lives and marine species [38–41]. It has been estimated that 940,000 child deaths occurred in 2016 alone worldwide because of polluted water consumption [42]. World Health Organization (WHO) projected that about 1.1 billion people globally drunk unsafe drinking water leading to about 3.1% of annual deaths [43]. Industrial water pollutions also put many marine species and water animals in endangered situations [44,45].

Desalination of sea/brackish has been considered as a potential solution for growing freshwater demands causing a considerable growth in the desalination industry in the past two decades [8–11]. Although sea/brackish water desalination has the ability to address the increasing fresh water demands, there are some major limitations associated with extensive usage of desalination systems. Current desalination technologies including reverse osmosis (RO), membrane desalination (MD), multiple-effect distillation (MED), electrodialysis (ED), electrodialysis reversal (EDR), ultrafiltation (UF) and nanofiltration (NF) have upper salinity limits beyond which they cannot treat the feedwater. Treating a concentrated rejected brine leaving a desalination system is a major problem. Concentrated brines have severe impacts on the environment and groundwater resources if not treated properly.

Economical costs associated with the brine treatment and/or disposal are very high today. ranging between 5 to 33% of total desalination cost [46]. The brine treatment and/or disposal costs depend on quality of concentrate, treatment level before disposal, type of disposal method used, and volume of concentrate handled [47].

Current brine disposal technologies include surface water discharge, sewer discharge, deep-well injection, evaporation ponds, and land applications. The surface water discharge method includes direct disposal of brine into oceans, seas, rivers, lakes and other water bodies [48,49]. This method is adopted by majority of the off-shore seawater desalination plants. However, a continuous discharge of highly concentrated brines into the shoreline results in significant disruption of the marine life environment. The increased salinity levels along the coastal line could also lead to an intensified problem of seawater intrusion into coastal groundwater aquifers [50]. The effects of brine disposal into coastal and marine environments can be alleviated by disposing the brines further offshore to the sea or diluting before disposal. To protect 99% of marine species, the brine should be diluted by a factor of 40-fold before disposal [51].

Application of the surface water discharge method is not a suitable option for inland brackish water desalination plants as inland water bodies contain high-quality water resources utilized for residential drinking applications. Sewer brine discharge method is a potential solution for inland desalination plants located near wastewater treatment plants. Here, brine leaving a desalination plant is treated by a waste water collection system [52]. The method, however, is only suitable for small-scale brackish water desalination plants

due to the potential adverse effect of high TDS rejected brines on the operation of waste water treatment plants [53]. High brine salinity levels hinder biological treatment processes employed in waste water treatment plants [54]. An alternative option for treatment of brine disposal in inland desalination plants is deep-well injection method. In the deep-well injection method, the brine is injected into a deep underground aquifer consisting of many layers of casting and grouting with impermeable rocks and clay [52,55]. The limiting factor of the deep-well injection method is pollution of surrounding water aquifers [56]. In addition, the deep-well injection method is not favorable at highly seismic locations due to the risk of groundwater pollution.

Evaporation ponds are shallowed, lined basins in which brine is allowed to slowly evaporate by utilizing natural solar heat energy [57]. Evaporation ponds, however, require large areas of land and high capital costs with a limited treatment capacity. Evaporation ponds have also environmental concerns of polluting soil and groundwater resources. Land application is a brine disposal method in which the brine is sprayed onto salt-tolerant plants and grass [52,58]. The land application is dependent on seasonal demand, climate conditions, and suitable land availability. Limitations associated with the land application method include soil and groundwater pollution, effect on surrounding vegetation, and brine storage and distribution.

Increased adverse effects associated with existing desalination techniques lead to imposition of new regulations on brine disposal [59,60]. The new regulations restrict usage of conventional brine discharge methods including the surface water discharge, deep-well

injection, land applications and evaporation ponds as they all have environmental concerns. The growing environmental concerns associated with current desalination systems have forced governments around the world to start imposing Zero Liquid Discharge (ZLD) regulations on chemical, pharmaceutical, and textile industries among others [16,61]. A ZLD system as its name implies eliminates liquid waste, thereby converting a brine stream into a high-quality water stream and solid wastes [62,63]. The solid waste rejected from a ZLD plant could be further processed for useful applications including salt production, and mineral extraction. The ZLD desalination of sea/brackish water bodies has the potential to limit industrial water pollution, thus being a promising solution for the growing global water demand [64–66].

1.2 Literature review

Early ZLD systems were standalone thermal systems. In these systems, the seawater is initially pretreated for pH adjustment reducing the scaling potential of metal pipes and heat

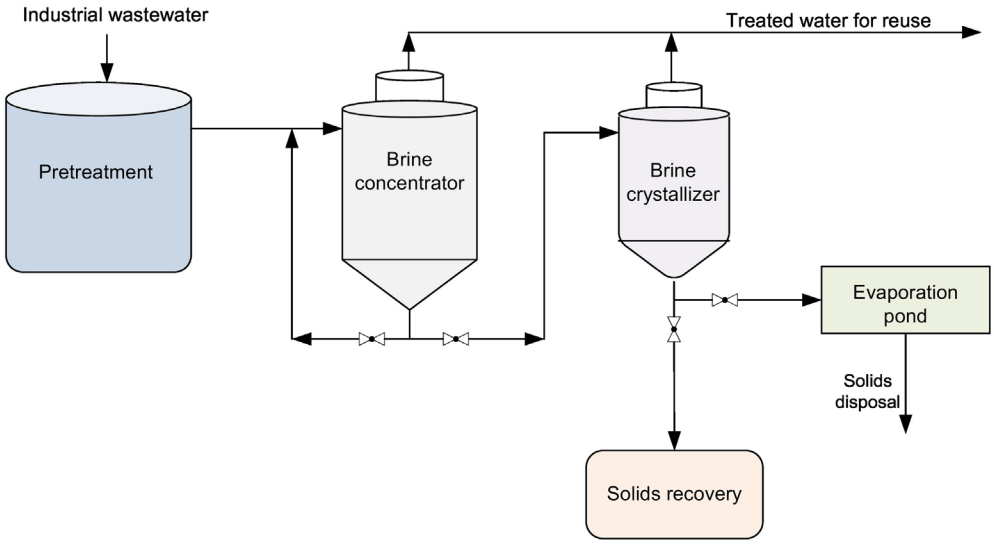

Figure 1.1. A schematic diagram of a thermal ZLD system (Copyright of Muhammad Yaqub et al. [18]).

exchangers utilized. The pH adjusted seawater is then evaporated in two core components called brine concentrator and brine crystallizer as shown in Fig.1.1 [16,18].

Brine concentrators generally employ a mechanical vapor compression process to evaporate the feed brine. A brine concentrator utilizes a bundle of vertical heat transfer tubes creating thin film evaporation on internal tube surfaces. Here, the feed brine mixed with recirculating brine slurry is pumped to top of the tube bundle for the internal thin film evaporation process. Formation of the thin films enhances the heat transfer rate, thereby reducing the compression ratio and energy consumption of compressor employed [67]. Calcium sulfate seeds are often added to avoid salt precipitation and subsequent scale formation on the heat transfer tubes [68,69]. The generated steam flows down in the same direction as the brine to the bottom of the brine concentrator through a concurrent thin film evaporation mechanism. The brine reaching the bottom sump recombines with the brine slurry as well as incoming feed and then again pumped to the top of the brine concentrator. The distillate vapor is passed through mist demisters for removal of any brine traces before entering a mechanical vapor compressor (MVC). The vapor compressor slightly increases the vapor pressure and pumps the distillate vapor to the shell side of the heat transfer tubes of brine concentrator. The superheated distillate vapor condenses on the outer surface of heat transfer tubes. The latent heat of the condensation process supplies latent heat required for thin film evaporation of the brine slurry flowing inside the tubes. The condensate water collected as the distillate product is then send to a heat exchanger to preheat the incoming feed. The typical energy consumption of the MVC brine concentrators are 20-39 kWh_e/m^3

of the distillate product [68,70]. A brine concentrator could treat feed waters to a salinity concentration of about 250,000 mg/L with recovery ratios of 90-98% with TDS values of less than 10mg/L [16]. The MVC brine crystallizers have high energy consumptions combined with high capital costs of expensive materials including titanium and stainless steel which are essential to prevent corrosion on heat transfer surfaces [69,71,72].

The concentrated brine rejected from the brine concentrator is sent to the brine crystallizer for complete water removal and salt crystallization formation processes. Similar to the brine concentrators, the brine crystallizers employ a mechanical vapor compression process for water evaporation. Vapor compression driven crystallizers usually operate in a forced circulation mode. In the forced circulation mode, the concentrated viscous brine is pumped and recirculated through submerged heat exchanger tubes at high pressures to avoid boiling and subsequent scaling/fouling on the tube surfaces [69]. The typical energy consumption of the brine crystallizers is as high as 52-66 kWh_e/m^3 of the

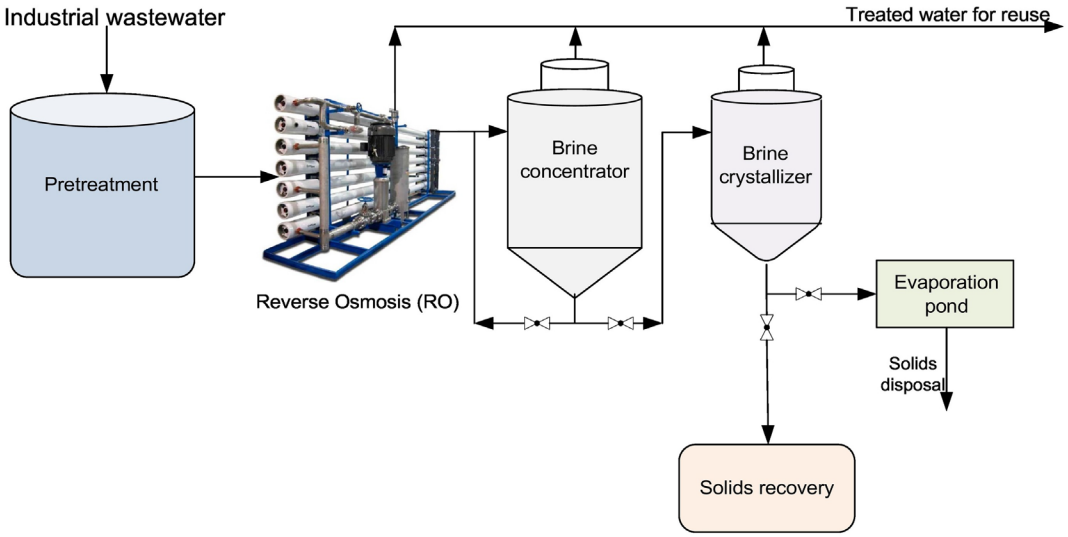

Figure 1.2. A schematic diagram of a RO incorporated ZLD system (Copyright of Muhammad Yaqub et al. [18]).

treated water [68]. This is almost three times of that of the brine concentrators. Although brine crystallizers consume a significant amount of energy, they are an integral part of a ZLD system due to limited alternative mechanisms for reliable treatment of brines with very high salinities and viscosities.

Evaporation ponds could be considered as a competitive alternative for brine crystallizers [73]. Evaporation ponds utilize natural solar energy to evaporate the water from the brine. In general, they are a viable alternative solution for treatment of small brine quantities at locations with high solar availability and inexpensive lands [74]. Despite of being highly energy efficient, there are major limiting factors hindering the extensive usage of evaporation ponds in ZLD systems. One such limiting factor is requirement of large area of land. In a hypothetical scenario of a ZLD desalination in Las Vegas, Nevada, the cost of land procurement excluding infrastructure was estimated to be three times that of the total cost associated with a brine concentrator followed by a brine crystallizer [75]. Another major concern with evaporation ponds is hazardous leakage of solid waste to the groundwater and environment [48,73,75–79].

Although brine concentrators and brine crystallizers are energy intensive, they are inevitable in large-scale economical ZLD systems where usage of evaporation ponds is not a viable option. Consequently, research in ZLD systems has focused on reducing volume of concentrated brine entering the brine crystallizers and concentrators. This could be achieved by appropriate pre-treatment processes. Reverse osmosis (RO), a well-established, pressure-driven, membrane-based desalination technique with excellent

energy efficiency has been incorporated into ZLD systems to reduce the energy consumption (cf. Fig. 1.2). Unlike the thermal processes, the feed in the RO systems does not need to undergo a phase change process, thereby decreasing the energy consumption of the system to a large extent.

The reverse osmosis process utilizes semi-permeable polymeric membranes with high selectivity for solvent molecules (i.e., pure water) while blocking solute molecules (i.e., dissolved salt ions). If the feed water and pure water are separated by such a membrane, flow naturally occurs from the high water potential side (i.e., low salt concentration) to the low water potential side (i.e., high salt concentration or feedwater), thus balancing the salt concentrations on both sides. By applying a pressure on the feedwater higher than the normal osmotic pressure, the flow will be reversed and pure water from the feedwater side flows towards the pure water side leaving concentrated feed on the feed side. The operating pressure for seawater desalination is around 55 to 68 bar [80]. The operating pressure for brackish water desalination will be less than that of seawater due to lower osmotic pressure caused by a lower feed salinity level. The typical energy consumption of a RO system for 50% recovery is 2 kWh_e/m^3 of the distillate product water which is much lower than that of brine concentrators and crystallizers [81]. Incorporating RO systems for pre-concentrating brine has showed 58-75% reduction in energy and 48-67% reduction in treatment cost compared to standalone brine concentrator combined with evaporation ponds based systems [82,83].

Although implementation of a RO system increases the overall system efficiency, there are several limiting factors and issues associated with the RO process. One such major issue is membrane fouling leading to (i) an increased required operating pressure, (ii) a reduction in water flux, and (iii) a decrease in membrane useful lifetime [84–87]. The fouling problem is more severe in ZLD systems compared to seawater and brackish reverse osmosis processes as the feed is concentrated to significantly higher levels in ZLD systems. To overcome the fouling problem in RO incorporated ZLD systems, extensive pre-treatment processes including chemical softening, pH adjustments, and ion-exchange need to be done. These pretreatment processes involve intensive use of chemicals which further produce solid waste as well as increased operational costs.

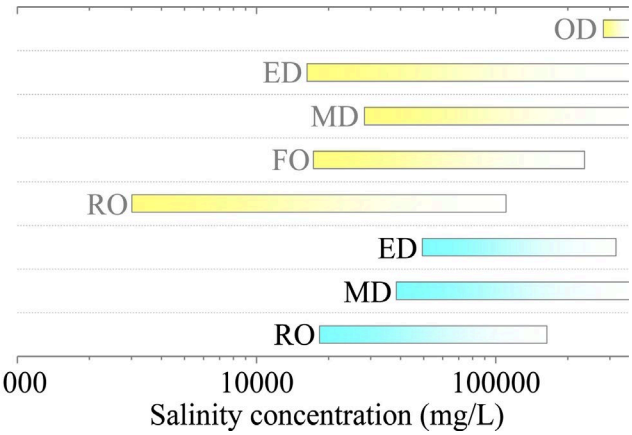

Figure 1.3. Salinity concentration limits of different desalination technologies (Copyright of Jheng- Han Tsai et al. [78]).

Furthermore, current RO modules cannot operate at very high operating pressures limiting the upper salinity limit of the RO brine to 75,000 mg/L [78]. This salinity is much lower than that of a brine concentrator (250,000 mg/L). This indicates that standalone RO systems cannot treat brines to the extent of a brine concentrator module. Therefore, a RO process is usually followed by a brine concentrator in RO incorporated ZLD systems [68,82]. Implementation of new desalination technologies such as membrane distillation, nano-filtration, ultra-filtration, electrodialysis, and forward osmosis among others into ZLD systems showed a pathway to pre-concentrate a feed water beyond the salinity limits of a RO system (cf. Fig. 1.3, and figure 1.4) [18,78,88–95]. A techno-economic comparison between membrane distillation (MD) and mechanical vapor compression in a ZLD system showed a 40% cost reduction compared to the MVC method [96].

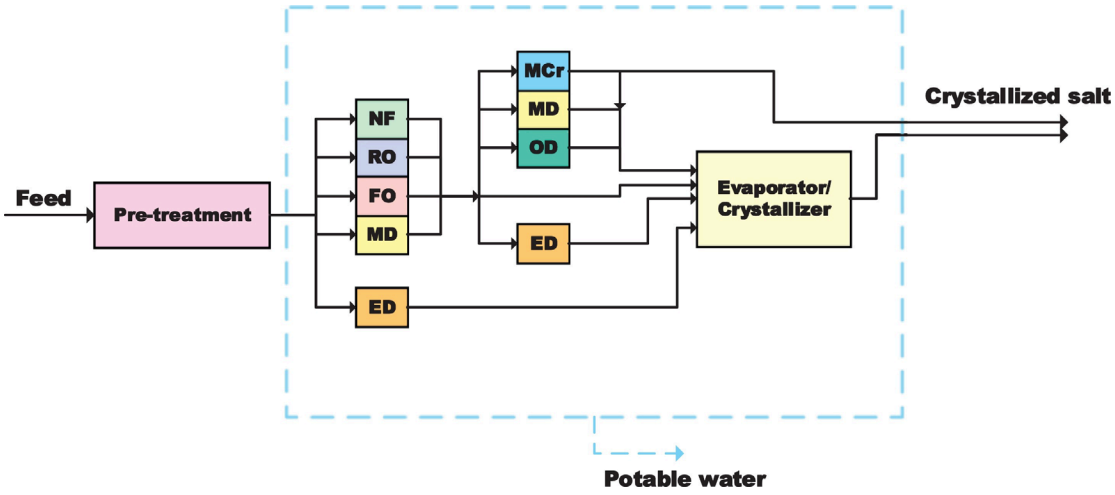

Figure 1.4. Different configurations of membrane-based ZLD systems (Copyright of Jheng-Han Tsai [78]).

A study reported by Kavithaa Loganathan et al. [97] demonstrated a pilot scale ZLD treatment of a basal aquifer water with high scaling/fouling potential and average TDS of 21,300 mg/L using a hybrid electrodialysis reversal (EDR) and reverse osmosis (RO)

followed by a brine crystallizer. Pre-treatment through sedimentation and ultrafiltration was found to be effective in removing suspended solids and turbidity. Further treatment of EDR-RO showed a recovery ratio of about 77% with concentrations up to 125,000mg/L followed by a brine crystallizer for near ZLD operation. In an another study, Kavithaa Loganathan et al. [98] reported a pilot scale ZLD system for treating basal water incorporated with RO and UF pretreatment processes. The UF pretreatment was found effective in removing suspended solids, as well as nearly 50% of oil and grease from the feed, thereby enabling the RO to operate at higher recovery ratios prior to evaporation-crystallization.

In a recent study, Kang Jia Lu et al. [99] demonstrated a novel design of a ZLD desalination system consisting of freeze desalination, membrane distillation followed by a crystallization unit. In this study, a modeled seawater with 3.5 wt% NaCl is considered. It was found that favorable operating conditions for a minimum overall energy consumption are a high feedwater temperature and concentration, a low distillate temperature and a large recovery ratio. Hanfei Guo et al. [100] simulated a flat sheet air gap membrane distillation coupled with an evaporative crystallizer for a ZLD water desalination treatment. Simulation results showed that NaCl mass fraction has a strong influence on system heat duty. The optimum operating condition with a minimum input energy was determined and the value of input energy was 1651.5 kJ/kg of product water. Guizi Chen et al. [101] investigated optimized operating parameters for a continuous membrane distillation crystallization (CMDC) zero liquid discharge process with 26.7% NaCl feed solution.

Their results showed that flowrates of the feed and permeate sides have a major impact on performance of the CMDC than temperatures of the feed and permeate sides. They also found that feed flowrate and temperature have a major influence on formed crystal size and distribution. Studies presented above only found ways to treat the brine efficiently before entering a crystallizer unit. None of them, however, were able to reduce energy consumption of the crystallization process.

An alternative emerging technology for treatment of concentrated brines is Wind Aided Intensified eVaporation (WAIV). WAIV is a thermal-based technology for evaporation of distillate from the brine slurry. In this technology, the concentrated brine is allowed to flow through densely packed wetted surfaces over which pressurized air is blown to evaporate the distillate from the brine. Oren et al. [102] developed a pilot scale model of WAIV to treat RO-EDR brines to the zero liquid discharge operation. Results showed that the WAIV unit produced final brines to a TDS of more than 300 mg/L and was able to recover mineral by-products such as magnesium salts. In another study, Macedonio et al. [103] studied the integration of a Reverse Osmosis - Membrane Crystallizer (RO-MCr) system with WAIV. The study reported that the system is able to reach a recovery ratio of 88.9% and limit the brine discharge to less than 0.27% of the feed. A full-scale demonstration of WAIV in Roma (Queensland) showed that the performance of WAIV is at least 10 times higher than the conventional evaporation ponds [104]. Although the WAIV technology enables to treat concentrated brines, water evaporated from a WAIV system cannot be harvested, thereby making no contribution to improvement of water recovery efficiency of the system.

The present thesis examines an alternative pathway substituting an energy-intensive MVC-driven brine crystallizer with an energy-efficient thermal vapor compression brine crystallizer concept. The proposed system relies on a high efficiency sorption-based ZLD distillation system to efficiently and economically distill water with high TDS content for mobile or semi mobile applications. The new ZLD system consists of a multi effect distillation (MED) unit embedded at the heart of a Lithium Bromide (LiBr) absorption-desorption system. The MED and LiBr units could exchange both heat and mass transfer processes. The system employs an absorption-based thermally-driven vapor compressor concept to pressurize vaporized brine of the ZLD unit from a low-pressure absorber to a high-pressure desorber environment. The vacuum environment required for the ZLD operation is established by the strong hygroscopic properties of aqueous LiBr salt. This eliminates the need for energy-intensive electrically-driven mechanical vapor compressors currently employed in advanced brine crystallizers. A detailed thermodynamic analysis of the system has been performed using a simultaneous equation solver called EES (Engineering Equation solver). Specific energy consumption, overall gained output ratio (GOR) and overall heat transfer coefficient of the system have been evaluated as a functions of recovery ratio (RR) of the MED unit, and number of the MED effects.

2 Concept

This research addresses the shortcomings inherent to current ZLD techniques by an innovative sorption-based concept in which a multiple-effect distillation (MED) unit is uniquely embedded at the heart of an absorption-desorption system. Contrary to current energy-intensive approaches, the proposed technology employs an absorption-based thermally-driven vapor compressor concept to create a low vapor pressure environment required for the ZLD treatment. Here, the ZLD operation is realized by the absorption process in which the brine discharged from the final MED effect is vaporized and then absorbed by a strong hygroscopic Lithium Bromide (LiBr) solution. The sub-atmospheric pressure of the crystallizer unit (4 kPa) at which both evaporation and absorption processes occur is determined by the equilibrium water vapor pressure of the LiBr solution. The desiccant solution is then pumped to a high-pressure desorber for subsequent desorption and condensation processes. This eliminates the need for energy-intensive electrically-driven mechanical vapor compressors currently employed in advanced brine crystallizers. In addition, the equilibrium temperature of the LiBr solution is almost 20-30°C higher than the equilibrium temperature of the brine slurry being vaporized for typical operating pressures. Despite the accompanying boiling point elevation, this temperature lift partially compensates the temperature drop between MED effects, thereby further improving the thermal desalination efficiency of the system.

Fig. 2.1 illustrates a detailed model of the proposed ZLD technology. The system consists of three main units: i) a forced-circulation (FC) ZLD unit, ii) a forward feed MED unit, and iii) an aqueous LiBr desorption unit. The ZLD unit is comprised of absorber, FC heat exchanger, and brine crystallizer modules. The thermal vapor compression process starts in the absorber module of the ZLD unit where the concentrated brine slurry leaving the last MED effect is vaporized and exothermically absorbed by the LiBr solution (cf. Fig. 2.1). Once the water vapor is absorbed, the weak LiBr solution is pumped from the ZLD unit to the desorption unit (DU). The water vapor is then endothermically desorbed and subsequently condensed and withdrawn from the system. Thermal energy required for the desorption process is supplied by an external heat source such as a hot steam line. The strong LiBr solution leaving the DU flows back to the absorber of the ZLD unit to complete the LiBr-water mixture loop.

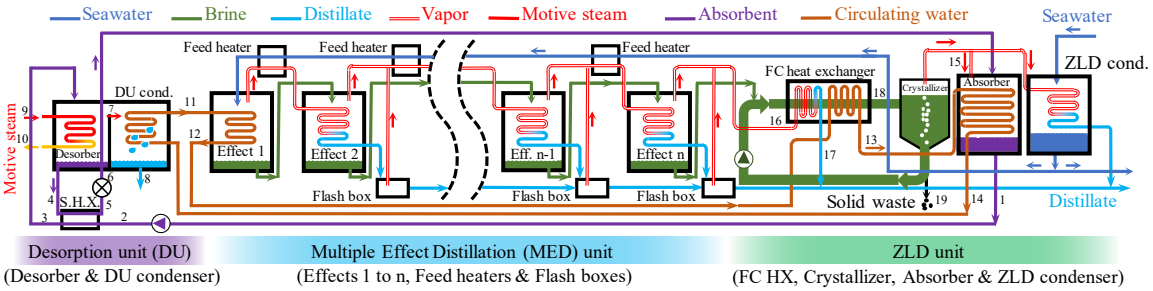

Figure 2. 1. A schematic diagram of the proposed sorption-based ZLD distillation system.

Latent heat released in the condenser module of the DU and absorption heat generated in the ZLD unit are collected by a closed thermal water loop to drive the first MED effect and FC heat exchanger. Latent heat associated with the condensing distillate vapor of each MED effect is successively utilized to drive subsequent MED effects. The vapor produced in the last MED effect is condensed in the forced-circulation brine heat exchanger. In the

ZLD unit, the brine slurry is circulated between the crystallizer maintained at a low vapor pressure and the FC heat exchanger operating at a high brine pressure. The low-pressure environment of the crystallizer module is established by the strong LiBr solution. A higher operating pressure of the brine heat exchanger minimizes scaling and clogging issues and allows superheating of the brine slurry. Here, the brine is concentrated beyond solubility limit of contaminants resulting in formation of salt crystals. Vaporized water is also absorbed into the LiBr solution to enable the ZLD operation which complete the sorption loop.

3 Thermodynamic modeling

A thermodynamic model of the system is developed using Engineering Equation Solver (EES) to evaluate energy consumption of the proposed technology. EES is a powerful simultaneous equation solver that includes a data base of the necessary thermophysical properties of working fluids employed in the system. The thermodynamic model includes the entire system shown in Fig. 2.1. The model developed by Mistry et al. [105] is used to formulate the MED sub-system. Seawater properties are estimated as a function of temperature and salinity [106,107]. Produced Distillate water is modeled as seawater with zero salinity. The vapor phase water properties are calculated using the Steam_IAPWS library in EES. EES uses IAPWS 1995 formulation for thermodynamic properties of ordinary water substance for general and scientific use [108].

The following assumptions are made to perform the thermodynamic modeling of the system:

1. All involved processes are assumed to be at steady-state.
2. Distillate water generated from the system is pure (i.e., the salinity of the distillate is (0 g/kg).
3. Seawater is incompressible and thermohydraulic properties are only functions of temperature and salinity.
4. Energy and pressure losses are negligible.
5. The solution leaving the absorber and desorber modules is at vapor-liquid equilibrium state.

Modeling of each individual component is described in details below.

3.1 Modeling of the ZLD unit

The operation of the ZLD unit is central to the proposed desalination system. Fig. 3.1 shows a schematic of the ZLD unit. The brine from the last MED effect (B_n) enters the FC heat exchanger to get super-heated beyond the saturation temperature of the brine crystallizer. The FC brine heat exchanger is heated by the condensing distillate vapor of the last MED effect and the closed water loop leaving the first MED effect. In the brine crystallizer, the brine becomes supersaturated by the LiBr solution absorbing the water vapor. Here, the excess solute results in formation of salt crystals that are continuously precipitated and removed from the brine slurry. The sub-atmospheric pressure of the brine crystallizer at which both evaporation and absorption processes occur is determined by the equilibrium water vapor pressure of the LiBr solution. The condensing distillate water in the FC brine heat exchanger (D_c^{FCHX}) is the sum of the distillate vapor generated in the last MED effect (D_n) and the flashed distillate vapor from the last flash box (D_{fb_n}).

$$D_c^{FCHX} = \dot{m}_{16} = D_n + D_{fb_n} \tag{3.1}$$

The net feed brine entering the crystallizer (F^{BC}) is equal to the brine leaving the last MED effect (B_n). Therefore, the total mass and salt balance equations for the brine crystallizer can be expressed as:

$$F^{BC} = B_n = B^{BC} + D^{BC} \tag{3.2}$$

$$F^{BC}X_F^{BC} = B^{BC}X_B^{BC} \tag{3.3}$$

where F^{BC} is the feed stream of the brine crystallizer, B^{BC} is the solid crystal salts rejected from the system, D^{BC} is the distillate vapor generated in the brine crystallizer, X_F^{BC} is the salinity of the feed entering, and X_B^{BC} is the salt concentration for a full distillated water removal process. At full ZLD operation, the recovery ratio (RR) defined as the desalinated water volume to the feed seawater volume is 95.6% (i.e., 100% ZLD operation).

The combined energy balance equation for the FC heat exchanger and the brine crystallizer modules can be written as:

$$D_c^{FCHX}\Delta h_{D_c}^{FCHX} + \dot{m}_{loop}C_{p,water}(T_{12} - T_{13}) = D^{BC}h_D^{BC} + B^{BC}h_B^{BC} - F^{BC}h_F^{BC} \tag{3.4}$$

where $\Delta h_{D_c}^{FCHX}$ is enthalpy changes of the condensing distillate vapor, h_D^{BC} is enthalpy of the distillate vapor generated in the crystallizer, h_B^{BC} is enthalpy of the salt crystals leaving the brine crystallizer, and h_F^{BC} is enthalpy of the feed brine entering the crystallizer.

The tube surface area of the FC heat exchanger (A^{FCHX}) can be also estimated as follows:

$$D_c^{FCHX}\Delta h_{D_c}^{FCHX} + \dot{m}_{loop}C_{p,water}(T_{12} - T_{13}) = U^{FCHX}A^{FCHX}\left(T_{in}^{FCHX} - T^{FCHX}\right) \tag{3.5}$$

where T_{in}^{FCHX} is the average tube-side temperature of the FC heat exchanger, and T^{FCHX} is the average shell-side temperature of the FC heat exchanger.

The Absorber module provides the partial vacuum environment required for the ZLD operation. Part of the distillate vapor generated in the brine crystallizer is absorbed by the strong LiBr solution and the remaining distillate vapor is condensed in the ZLD condenser module (cf. Fig. 3.1). The heat of the exothermic absorption process is collected by the closed thermal water loop. The amount of water vapor absorbed by the LiBr solution ($\emptyset D^{BC}$) is defined by the heat required for the first MED effect and the ZLD unit.

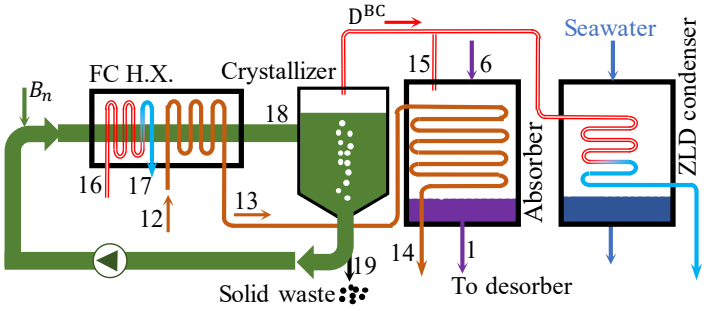

Figure 3. 1. A schematic of the ZLD unit consisting of the FC heat exchanger, brine crystallizer, absorber, and ZLD condenser modules.

The mass balance equations between the streams of the absorber can be written as:

$$\dot{m}_{15} = \emptyset D^{BC} \tag{3.6}$$

$$\dot{m}_1 = \dot{m}_{15} + \dot{m}_6 \tag{3.7}$$

$$\dot{m}_1 x_1 = \dot{m}_6 x_6 \tag{3.8}$$

where $\dot{m}_{15}$ is mass flowrate of the distilled vapor absorbed by the LiBr solution, and $\emptyset$ is mass fraction of the distillate vapor absorbed. Here, $\dot{m}_1$ is mass flowrate of the LiBr solution leaving the absorber module, $\dot{m}_6$ is mass flowrate of the LiBr solution entering the absorber module, and x_1 and x_6 are their respective LiBr concentration values.

Similarly, the energy balance equations between the streams entering and leaving the absorber module can be written as:

$$\dot{Q}_a = -\dot{m}_1 h_1 + \dot{m}_{15} h_{15} + \dot{m}_6 h_6 \tag{3.9}$$

$$\dot{Q}_a = \dot{m}_{loop} C_{p,water} (T_{14} - T_{13}) \tag{3.10}$$

$$\dot{Q}_a = UA_a \left((T_6 - T_{14}) - (T_1 - T_{13})\right) / \left(ln \frac{T_6 - T_{14}}{T_1 - T_{13}}\right) \tag{3.11}$$

where $\dot{Q}_a$ is heat of the absorption process, h_1 is enthalpy of the LiBr solution leaving the absorber, h_{15} is enthalpy of the distillate vapor absorbed, and h_6 is enthalpy of the LiBr solution entering the absorber module. In addition, T_{13} and T_{14} are temperatures of the cooling water loop entering and leaving the absorber module, respectively.

The remaining distillate vapor produced in the ZLD unit ($(1 - \emptyset) D^{BC}$) is condensed in the ZLD condenser module cooled by the feed seawater. Usually excess seawater is required for handling the cooling load of the condenser. From the seawater, required feed is sent to the MED unit as feed and the remaining excess seawater is rejected back to the seawater source. The condensed distillate vapor is then removed as the product distillate water. The energy balance equations for the ZLD condenser

$$(1 - \emptyset) D^{BC} \Delta h_D^{BC} = \dot{m}_{sw} (h_{sw}^{out} - h_{sw}^{in}) \tag{3.12}$$

$$\dot{m}_{sw} (h_{sw}^{out} - h_{sw}^{in}) = U^{Cond} A^{Cond} \left(\mathrm{T_{sw}^{out}} - \mathrm{T_{sw}^{in}}\right) / \left(\ln \frac{T_D^{BC} - \Delta h_{sw}^{in}}{T_D^{BC} - \Delta h_{sw}^{out}}\right) \tag{3.13}$$

where Δh_D^{BC} is the latent heat of evaporation of the distillate vapor, $\dot{m}_{sw}$ is mass flowrate of the seawater required for condensation, U^{Cond} is the condenser overall heat transfer coefficient, and A^{Cond} is area of the ZLD condenser. In addition, h_{sw}^{in}, and h_{sw}^{out} are enthalpies of the seawater at the inlet and outlet of the condenser module, respectively.

3.2 Modeling of the desorption unit

A schematic of the desorption unit (DU) is depicted in Fig. 3.2. The weak LiBr solution leaving the absorber module is pumped to the desorption unit in which the strong desiccant solution is regenerated. A hot condensing steam line supplies the heat required for the water vapor rejection process. The cold weak and the hot strong LiBr solution streams exchange heat in a solution heat exchanger positioned between the absorber and desorber modules, thereby reducing desorber heat input. The desorbed water vapor is condensed in the DU condenser module. The latent heat of the condensation process is collected by the closed water circulation loop before entering the first MED effect. The condensed distillate water is continuously withdrawn from the system. The mass and concentration balance equations of the desorption unit can be summarized as:

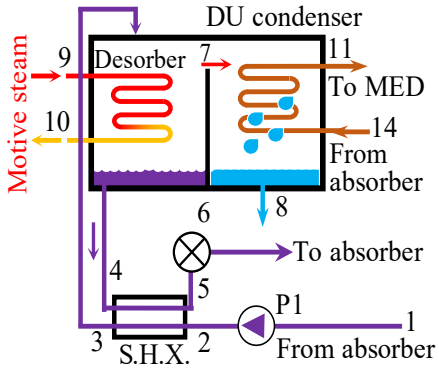

Figure 3. 2. A schematic of the desorption unit.

$$\dot{m}_1 = \dot{m}_2 = \dot{m}_3, \dot{m}_4 = \dot{m}_5 = \dot{m}_6, \dot{m}_3 = \dot{m}_4 + \dot{m}_7, \dot{m}_7 = \dot{m}_8 \tag{3.14}$$

$$x_1 = x_2 = x_3, x_4 = x_5 = x_6 \tag{3.15}$$

$$\dot{m}_3 x_3 = \dot{m}_4 x_4 \tag{3.16}$$

where $\dot{m}_i$ and x_i represent mass flowrate and LiBr concentration, respectively.

The energy balance equations across individual components of the desorption unit are expressed as:

$$\dot{w}_{pump} = v_1(p_2 - p_1) = \dot{m}_2 h_2 - \dot{m}_1 h_1 \tag{3.17}$$

$$h_5 = h_6 \tag{3.18}$$

$$\dot{Q}_{shx} = \dot{m}_2(h_3 - h_2) = \dot{m}_4(h_4 - h_5) \tag{3.19}$$

$$= U^{shx} A^{shx} ((T_4 - T_3) - (T_5 - T_2))/(ln\frac{T_4 - T_3}{T_5 - T_2})$$

$$\dot{Q}_d = -\dot{m}_3 h_3 + \dot{m}_4 h_4 + \dot{m}_7 h_7 = \dot{m}_9 h_{fg} = \tag{3.20}$$

$$U^d A^d ((T_9 - T_4) - (T_{10} - T_7))/(ln\frac{T_9 - T_4}{T_{10} - T_7})$$

$$\dot{Q}_{DU-cond} = \dot{m}_7 h_7 - \dot{m}_8 h_8 = \dot{m}_{loop} C_{p,water}(T_{11} - T_{14}) \tag{3.21}$$

$$= (UA)^{DU-cond} ((T_8 - T_{14}) - (T_8 - T_{11}))/(ln\frac{T_8 - T_{14}}{T_8 - T_{11}})$$

where $\dot{w}_{pump}$, $\dot{Q}_{shx}$, $\dot{Q}_{d}$, $\dot{Q}_{DU-cond}$, h_i, and h_{fg} are work input of the pump, heat exchanged in the solution heat exchanger, heat exchanged in the desorber module, heat exchanged in the condenser module, enthalpy, and enthalpy of condensation respectively.

3.3 Modeling of the MED unit

Effect is the primary component of the MED unit. Fig. 3.3 shows a schematic of a MED effect indicating incoming and outgoing streams. In each effect, an incoming feed brine (F) is partially vaporized dividing the feed stream into a concentrated brine (B) and a distillate vapor (D) stream. The thermal energy required for the evaporation process is supplied by latent heat of condensing distillate vapor (D_c) generated in the preceding effect. Since the operating pressure of each effect is slightly below the saturation pressure, the distillate vapor generated in each effect is a combination of flash evaporation (D_f) and boiling (D_b). The portion of the feed brine before the boiling process is called the brine within effect (B_{we}). Therefore, a portion of the brine within each effect is vaporized forming the distillate due to boiling (D_b) and the concentrated brine (B). The mass and salt balance equations between the incoming and outgoing streams can be written as:

$$F = B + D \tag{3.22}$$

$$D = D_f + D_b \tag{3.23}$$

$$F = B_{we} + D_f \tag{3.24}$$

$$FX_F = BX_B \tag{3.25}$$

$$FX_F = B_{we}X_{B_{we}} \tag{3.26}$$

where F, B, D, B_{we}, D_f and D_b are mass flowrates of the brine feed entering the effect, the brine leaving the effect, the distillate vapor generated in the effect, the brine within the effect, the distillate vapor generated by flash evaporation and the distillate vapor generated by boiling, respectively. Also, X_F, X_B and $X_{B_{we}}$ are salinity of the feed, the brine leaving the effect and the brine within the effect, respectively.

The energy balance equations between the streams entering and leaving each effect can be also expressed as:

$$D_c\Delta h_{D_c} + Fh_F = Dh_D + Bh_B \tag{3.27}$$

$$Fh_F = B_{we}h_{B_{we}} + D_f h_{D_f} \tag{3.28}$$

where D_c is mass flow rate of the condensing distillate entering the effect, Δh_{D_c} is enthalpy changes of the condensing distillate, h_D is enthalpy of the distillate vapor generated in the effect, h_B is enthalpy of the brine leaving the effect, h_F is enthalpy of the feed entering the effect, $h_{B_{we}}$ is enthalpy of the brine within the effect, and h_{D_f} is enthalpy of the distillate generated due to flashing. It should be mentioned that there is no flash evaporation associated with the first effect ($D_{f,\ 1st\ effect}$=0) since the feed seawater brine entering the first effect is at a subcooled condition. In addition, the heat required for evaporation of the feed

brane of the first effect is supplied by the closed water circulation loop. Therefore, the energy balance for the first effect can be modified as:

$$\dot{m}_{loop} C_{p,water} (T_{11} - T_{12}) = D_1 h_{D_1} + B_1 h_{B_1} - F_1 h_{F_1} \quad (3.29)$$

where $\dot{m}_{loop}$ is mass flowrate of the water circulation loop, $C_{p,water}$ is the specific heat of water, T_{11} is the temperature of water entering the first effect, and T_{12} is the temperature of water leaving the first effect.

The required tube surface area (A_e) of each effect for complete in-tube condensation can be calculated considering the temperature difference driving the condensation process between the tube ($T_{D_{sat}}^{prev}$) and shell (T_e) sides as follows:

$$D_c \Delta h_{D_c} = U^e A^e (T_{D_{sat}}^{prev} - T_e) \quad (3.30)$$

where $T_{D_{sat}}^{prev}$ is the saturation temperature of the distillate from the previous effect, T_e is the temperature of the effect, and U_e is the overall heat transfer coefficient.

In the flash box (cf. Fig. 3.3), the effect condensed distillate (D_c) and condensed distillate from the previous effects (D_{bd}^{in}) are mixed. Here, the mixed condensed distillate is depressurized to its current effect pressure (p_e) in which a part of the incoming distillate stream is then flash vaporized (D_{fb}). As shown in Fig. 3.3, the flashed distillate vapor leaving the flash box and the distillate vapor generated in the current effect are mixed in the feed heater before being condensed in the next effect. The remaining condensed distillate (D_{bd}) is also blown out to the next flash box. The mass and energy balance equations for the flash box can be expressed as:

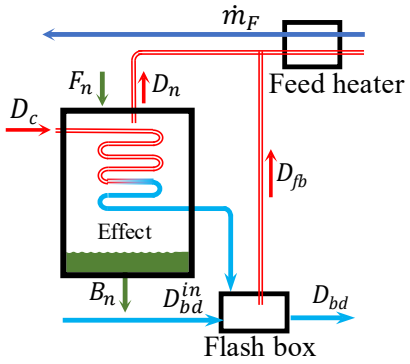

Figure 3. 3. A schematic of the MED effect consisting of a MED effect, a flash box, and a feed heater.

$$D_c + D_{bd}^{in} = D_{fb} + D_{bd} \tag{3.31}$$

$$D_c h_{D_c} + D_{bd}^{in} h_{bd}^{in} = D_{fb} h_{D_{fb}} + D_{bd} h_{D_{bd}} \tag{3.32}$$

where h_{D_c}, h_{bd}^{in}, $h_{D_{fb}}$, and $h_{D_{bd}}$ are enthalpies of the condensed distillate from the current effect, the distillate blown in from the previous flash box, the distillate flashed vaporized in the current flash box, and the distillate blown out from the current flash box, respectively.

Feed heaters (cf. Fig. 3.3) recover heat and thus reduce thermal energy required in the first MED effect. Here, heat released by a partial condensation of the distillate vapor from the effect and the flashed distillated vapor from the flash box is supplied to the feed seawater. A terminal temperature difference of 5°C is considered to define amount of heat

transferred between the streams. The energy balance between the seawater and the distillate vapor in the feed heater can be written as:

$$(D + D_{fb})(h_{D_c}^{in} - h_{D_c}^{out}) = \dot{m}_F(h_{\dot{m}_F}^{out} - h_{\dot{m}_F}^{in}) \tag{3.33}$$

$$(D + D_{fb})(h_{D_c}^{in} - h_{D_c}^{out}) = U^{FH}A^{FH}\,(T_{\dot{m}_F}^{in} - T_{\dot{m}_F}^{out})\Big/(ln\frac{T_{D_{c,sat}} - T_{\dot{m}_F}^{out}}{T_{D_{c,sat}} - T_{\dot{m}_F}^{in}}) \tag{3.34}$$

where $h_{D_c}^{in}$ is enthalpy of the distillate vapor entering the feed heater, $h_{D_c}^{out}$ is enthalpy of the distillate vapor leaving the feed heater, $\dot{m}_F$ is mass flowrate of the feed entering the feed heater, $h_{\dot{m}_F}^{in}$ is enthalpy of the feed seawater entering the feed heater, and $h_{\dot{m}_F}^{out}$ is enthalpy of the feed seawater leaving the feed heater.

To validate the developed thermodynamic model, results obtained from the MED unit is compared against those of Mistry et al. [105]. For the validation purpose, input parameters provided to the present model are similar to Mistry et al. [105]. Results compared at different operating conditions showed an excellent agreement with a maximum deviation of less than 2%. The slight difference in results were rooted in estimation of brine properties at high salinity levels. Fig. 3.4 showing performance ratios obtained from the present model and those of Mistry et al.

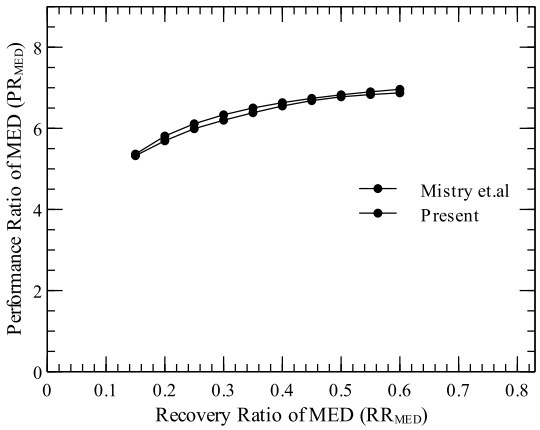

Figure 3. 4. A comparison between performance ratios of the present model with those of Mistry et al. [105].

[105] indicates an excellent agreement at different recovery ratios.

4 Results and Discussion

The thermodynamic model discussed above is employed to understand energy performance and size of the proposed sorption-based ZLD desalination system (i.e., thermal comp.) at different thermodynamic conditions and recovery ratios. Performance metrics of the proposed system are also studied at different number of MED effects to optimize system configuration. In addition, the results are compared against a MED system coupled with a FC heat exchanger achieving the ZLD operation through thermal evaporation alone (i.e., thermal evap.). Table 4.1 summarizes fixed input parameters considered for the thermodynamic modeling.

Table 4. 1 Fixed input parameters considered for the thermodynamic modeling.

Parameter	**Value**
Brine crystallizer operating temperature, T^{BC}	29.25°C
Seawater temperature at the inlet of the ZLD condenser, T_{sw}^{in}	23°C
Seawater temperature at the outlet of the ZLD condenser, T_{sw}^{out}	27°C
Temperature difference b/w MED effects, TTD_e	3.75°C
Minimum terminal temperature difference b/w streams in feed heater, TTD_{FH}	5°C
Mass flow rate of the feed seawater, $\dot{m}_F$	2.5 kg/s
Salinity of the feed, X_F	42 g/kg
Effectiveness of the solution heat exchanger, ε	0.8

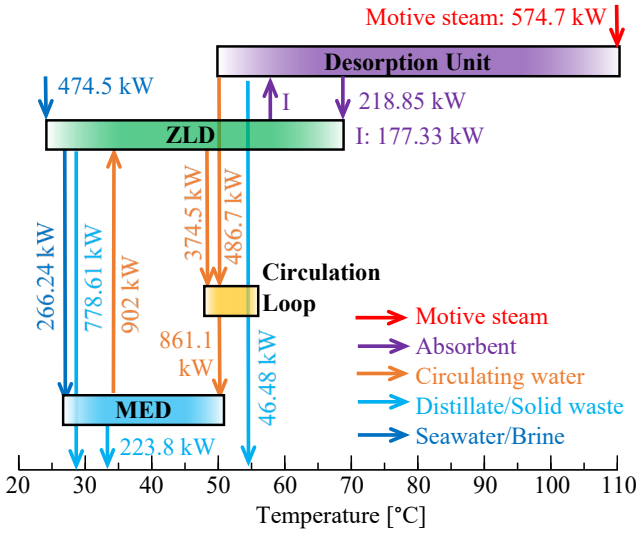

Figure 4. 1. Overall energy flow and respective unit temperature ranges of the proposed sorption-based ZLD system with six MED effects at a MED recovery ratio of 80%.

Fig. 4.1 shows overall energy flow of the proposed sorption-based ZLD system with six MED effects at a MED recovery ratio of 80%. As shown, the system accepts 574.7 kW of thermal energy at 113°C (i.e., T_9) to regenerate the LiBr solution in the desorber module, and rejects the same net energy (through distillate in MED, ZLD, and desorption units minus the feedwater). It also shows the operating temperature range of each unit of the system. Table 4.2 summarizes detailed operating conditions of the system shown in Fig. 4.1. The water vapor generated during the desorption process (i.e., point 7) condenses at a temperature of 89.9°C in the DU condenser module. The 486.7 kW latent heat of the condensation process is harvested by the closed water circulation loop rising its temperature to 52.75°C (i.e., T_{11}). The closed water loop delivers 861 kW thermal energy to the first MED effect generating distillate vapor at a temperature of 51.75°C (i.e., T_{D1}). The latent heat of the condensing distillate vapor generated in each MED effect drives the

next MED effect. The brine leaving the last MED effect at a temperature of 33°C enters the FC heat exchanger and the brine crystallizer to get vaporized and thus achieve the ZLD operation. The latent heat required for the brine vaporization in the crystallizer module operating at a temperature of 29.25°C (i.e., T_{18}) is supplied by the FC heat exchanger. The condensing distillate vapor of the last MED effect and the closed water circulation loop provide the heat input of the FC heat exchanger. Capturing the distillate vapor produced in the ZLD unit (i.e., point 15), the strong LiBr solution leaving the desorber module (i.e., T_6) establishes the ZLD operating pressure of 4.067 kPa. The example shown here utilizes a total energy consumption of 66.65 kWh_{th}/m^3 of treated water to achieve a complete ZLD operation.

Table 4. 2 Operating conditions of the proposed sorption-based ZLD system with six MED effects at a MED recovery ratio of 80%.

Unit	**Module**	**Point**	**T [°C]**	**P [kPa]**	**ṁ [kg/s]**	**X_{brine} or x_{LiBr}**
Desorption unit	Desorber (Q = 574.7 kW)	9 (Motive steam)	113	-	0.2587	-
		10 (Motive steam)	113	-	0.2587	-
		3 (LiBr)	91.15	16.15	1.291	0.5418
		4 (LiBr)	112.50	16.15	1.091	0.6411
		7 (Water vapor)	89.91	16.15	0.2	0 g/kg
	Condenser (Q = 486.7 kW)	8 (Liquid water)	55.50	16.15	0.2	0 g/kg
		11 (Closed loop)	52.75	-	102.5	-
	Solution HX (Q = 84.53 kW)	2 (LiBr)	60	16.15	1.291	0.5418
		5 (LiBr)	70.50	16.15	1.091	0.6411
ZLD unit	Absorber (Q =552.2 kW)	6 (LiBr)	70.50	4.067	1.091	0.6411
		1 (LiBr)	60	4.067	1.291	0.5418
		13 (Circ. loop)	50.34	-	102.5	-

		14 (Circ. loop)	51.62	-	102.5	-
	Crystallizers	15 (Water vapor)	29.25	4.067	0.2	0 g/kg
		18 (Brine slurry)	29.25	4.067	0.5	210 g/kg
		19 (Solid salt)	29.25	4.067	0.105	Pure salt
	FC HX (Q = 987.5 kW)	16 (Water vapor)	33	5.035	0.3337	0 g/kg
		17 (Liquid water)	33	5.035	0.3337	0 g/kg
		12 (Circ. loop)	50.75	-	102.5	-
MED unit	Effect 1 (Q = 861.1 kW)	Feed brine, F_1	46.75	13.47	2.5	42 g/kg
		Distillate vapor, D_1	51.75	13.47	0.3411	0 g/kg
	Effect 2 (Q = 775.3 kW)	Feed brine, F_2	51.75	13.47	2.159	48.64 g/kg
		Distillate vapor, D_2	48	11.18	0.3382	0 g/kg
	Effect 3 (Q = 776.7 kW)	Feed brine, F_3	48	11.18	1.821	57.67 g/kg
		Distillate vapor, D_3	44.25	9.231	0.3354	0 g/kg
	Effect 4 (Q =778.2 kW)	Feed brine, F_4	44.25	9.231	1.485	70.69 g/kg
		Distillate vapor, D_4	40.5	7.584	0.3326	0 g/kg
	Effect 5 (Q = 779.7 kW)	Feed brine, F_5	40.5	7.584	1.153	91.09 g/kg
		Distillate vapor, D_5	36.75	6.197	0.3298	0 g/kg
	Effect 6 (Q = 771.2 kW)	Feed brine, F_6	36.75	6.197	0.8229	127.6 g/kg
		Distillate vapor, D_6	33	5.035	0.3229	0 g/kg

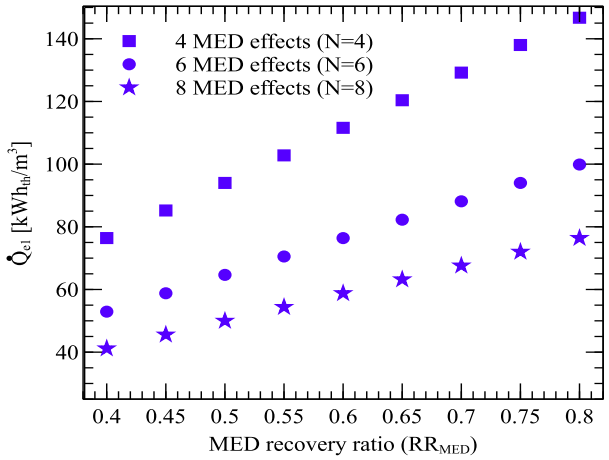

Figure 4. 2. Specific thermal energy of the first MED effect versus MED recovery ratio at different and number of MED effects

Fig. 4.2 shows specific thermal energy required for the first MED effect of the proposed sorption-based ZLD system as a function of the MED recovery ratio (i.e., RR_{MED} or recovery ratio associated with the MED unit) at different numbers of MED effects. As shown, required thermal energy of the first MED effect increases as amount of high purity water produced increases (i.e., higher RR_{MED}) at a particular number of MED effects. This is attributed to greater amount of distillate vapor generated at higher recovery ratios of the MED unit, thus requiring additional input thermal energy for the evaporation process. In addition, at a fixed recovery ratio, thermal energy of the first MED effect per unit of distillate water produced decreases as number of the MED effects increases. This is because the latent heat of the condensing distillate vapor is successively recovered through a larger number of the MED effects, thereby reducing the input thermal energy of the first MED effect.

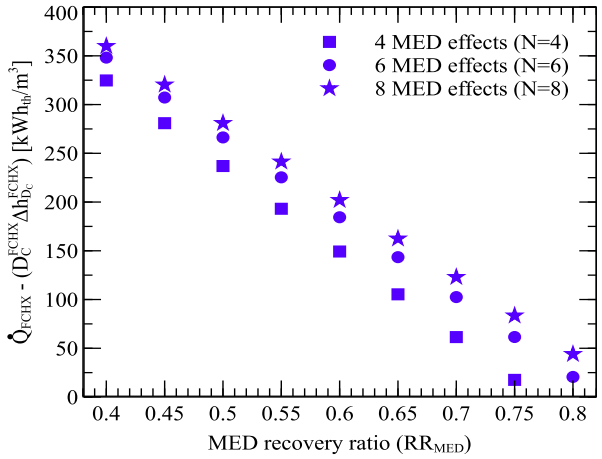

Figure 4. 3. Additional specific thermal energy required for the ZLD treatment at different MED recovery ratios and number of MED effects

The brine leaving the last MED effect enters the FC heat exchanger and brine crystallizer modules to be fully desalted. The specific thermal energy required for the ZLD treatment is partially supplied by the latent heat of the condensing distillate vapor leaving the last MED effect. However, this heat is typically not sufficient for full vaporization of the brine slurry of the ZLD unit. Fig. 4.3 shows additional specific energy needed for a complete ZLD operation at different MED recovery ratios and number of MED effects. As shown, additional thermal energy of the ZLD unit per unit of the purified water generated decreases as recovery ratio of the MED unit increases. Amount of the feed seawater vaporized in the MED unit increases at higher recovery ratios, thereby decreasing required thermal evaporation load of the ZLD unit. Furthermore, additional specific thermal energy required for the ZLD treatment increases when the number of the MED effect increases. This is attributed to thermal energy exchanged per MED effect, which decreases as the number of the MED effects increases. This in turn reduces thermal energy supplied by the last MED effect, thereby increasing external energy needed for the ZLD unit.

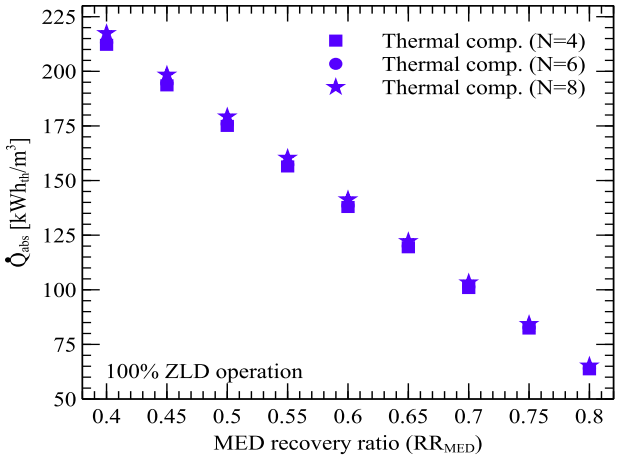

Figure 4. 4. Specific heat released during the absorption process at different recovery ratios of the MED unit.

The water vapor produced in the ZLD crystallizer is partially absorbed by the strong LiBr solution of the absorber module. The absorbed water vapor is then thermally rejected in the desorption unit and subsequently condensed. Both heat generated during the absorption process and latent heat released in the condenser module of the DU are collected by the closed water circulation loop to supply additional thermal energy required for the ZLD treatment in the crystallizer module and evaporation in the first MED effect. Fig. 4.4 shows heat produced during the absorption process per unit of the desalinated water generated at different MED recovery ratios. As mentioned, thermal vaporization load of the brine crystallizer decreases at higher recovery ratios of the MED unit. This in turn decreases amount of vapor absorbed by the LiBr solution, thereby reducing heat of the absorption process. It should be mentioned that the above trend is independent of the number of the MED effects and only depends on recovery ratios of the MED unit.

Fig. 4.5 shows total thermal energy required by the proposed thermal compression based ZLD system per unit of the desalinated water produced at different MED recovery ratios. This thermal energy is supplied to the desorber module of the system. It is evident that required specific thermal energy of the proposed thermal compression system decreases as recovery ratio of the MED unit increases. This is because the additional energy required for the ZLD operation (cf. Fig. 4.3) significantly declines with the MED recovery ratio, thereby decreasing the total input thermal energy of the system at higher values of RR_{MED}.

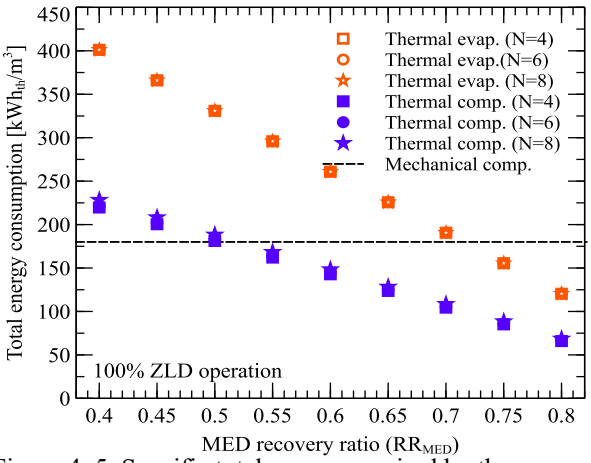

Figure 4. 5. Specific total energy required by the proposed ZLD system at different MED recovery ratios.

In addition, Fig. 4.5 shows specific thermal energy required by a multiple-effect thermal evaporation approach to achieve the ZLD operation for reference. In the thermal evaporation approach, the brine leaving the last MED effect is sent to a thermally driven FC heat exchanger module to be fully vaporized and then condensed by the cooling effect of the feed seawater (i.e., no absorber modules included). Furthermore, Fig. 4.5 illustrates performance of the electrically-driven mechanical vapor compressors (i.e., mechanical compression) utilized in advanced ZLD brine crystallizers. A site-to-source energy

conversion ratio of 3.06 with a combined power generation and transmission efficiency of 32.6% is used to estimate an equivalent thermal energy consumption. Consuming an electric energy range of 52-66 kWh_e/m^3, state-of-the-art mechanical compression based ZLD systems have an equivalent thermal energy usage of 160-200 kWh_{th}/m^3 [16]. As shown, required specific thermal energy of the proposed thermal compression system is significantly lower than that of both thermal evaporation and mechanical compression based ZLD approaches owing mainly to the recovery of the heat generated by the ZLD absorber and DU condenser modules.

Fig. 4.6 shows gained output ratio (GOR) of the proposed ZLD desalination system and a thermal evaporation based ZLD approach at different MED recovery ratios. The GOR representing the first law efficiency of a desalination plant is defined as heat required to evaporate the product water to that of the system input. As shown, the GOR of the proposed ZLD system increases at higher recovery ratios of the MED unit. This is attributed to the total input thermal energy to the system (cf. Fig. 4.5), which decreases as recover ratio of the MED unit increases. In addition, the GOR of the proposed ZLD system is significantly higher than that of the thermal evaporation based ZLD approach (e.g., 10 versus 5.5 at a MED recovery ratio of

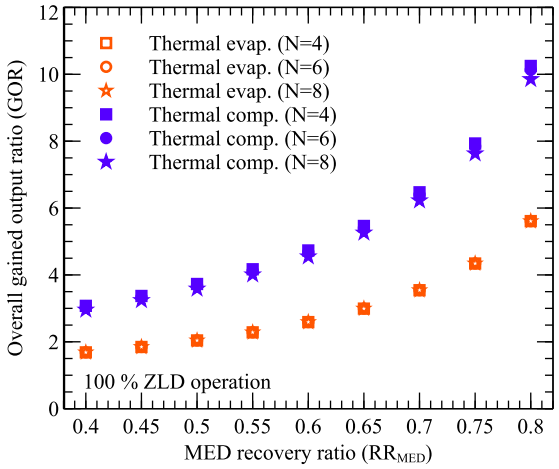

Figure 4. 6. Overall gained output ratio of the proposed ZLD system at different MED recovery ratios.

80%) mainly due to the difference existing between their input energy levels (cf. Fig. 4.5). It can be also seen that the GOR of both thermal compression and evaporation systems achieving the ZLD operation are insensitive to the number of MED effects.

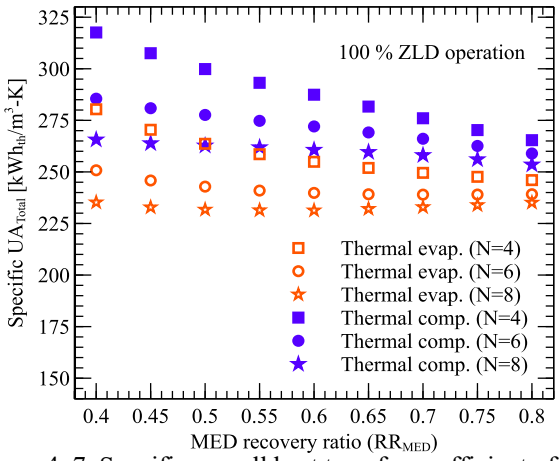

Figure 4. 7. Specific overall heat transfer coefficient of the proposed ZLD system at different MED recovery ratios

Fig. 4.7 depicts required overall heat transfer coefficient (i.e., UA) of the proposed ZLD system per unit of the distillate water produced at different MED recovery ratios. While the GOR represents operating expense (OPEX) of a desalination plant, the specific overall UA indicates capital expenditure (CAPEX) of a system. As shown, for a fixed recovery ratio, the specific overall UAs required by the proposed ZLD system and the thermal evaporation based ZLD approach decrease as number of the MED effects increases. This is mainly because of a fixed logarithmic mean temperature difference (LMTD) assumed across each MED effect (cf. Table 4.1), which increases the overall LTMD across the MED unit as number of the MED effects increases. This in turn reduces the overall required UA per unit of product water. In addition, the specific overall UA decreases at higher recovery ratios of the MED unit. This can be attributed to the required overall UAs of the ZLD and

desorption units, which decrease as recovery ratio of the MED unit increases. Furthermore, the specific overall UA of the proposed sorption-based ZLD system is higher than that of the thermal evaporation based ZLD approach mainly due to the additional heat transfer area required by the absorber and desorber modules.

5 Future Scope

The present thermodynamic analysis showed the promise of the proposed sorption-based ZLD system in reducing total energy consumption. As discussed, the thermal compression process could significantly lower required input energy for the ZLD treatment compared to that of the thermal evaporation and MVC-driven ZLD systems. The system performance can be further enhanced by desiccant rejection at higher temperatures. This enables the ability to harvest higher exergies available at higher temperatures. This can be achieved through desorbing the distillate vapor in multiple stages in contrast to a single-stage desorption unit. There are two possible configurations for multiple stage desorption, series and parallel. Uplifting of the operating temperature is a major problem in conventional thermal desalination systems due to scaling/fouling issue on heat exchanger surfaces. Scale formation increases thermal resistances thereby increasing operational cost of the system. Implementing the current design enables a way to uplift the operating temperatures by bypassing the scaling issue. Furthermore, the proposed technology could be furthered evaluated through careful experimental testing.

6 Conclusion

A novel desiccant-based ZLD desalination system in which a MED unit is uniquely embedded at the heart of an absorption-desorption system was introduced. The new system eliminates the need for energy-intensive electrically-driven mechanical vapor compressors currently utilized in state-of-the-art ZLD brine crystallizers. Thermal performance of the proposed ZLD system was comprehensively analyzed through a detailed thermodynamic modeling at various thermohydraulic conditions. Major conclusions drawn from the present study include:

- The proposed ZLD system employing the strong hygroscopic properties of the aqueous LiBr salt is able to harvest the heat generated by the ZLD absorber and DU condenser modules.
- Thermal energy consumption of the new thermal compression based ZLD system is significantly lower than that of both thermal evaporation and mechanical compression based ZLD approaches.
- The overall GOR of the proposed ZLD system is substantially higher than that of the thermal evaporation based ZLD approach (e.g., 10 versus 5.5 at a MED recovery ratio of 80%).
- Overall UA of the proposed sorption-based ZLD system per unit of the product water is higher than that of the thermal evaporation based ZLD approach mainly due to the additional heat transfer area required by the absorber and desorber modules.

In summary, the present study confirms that the sorption-based thermal compression technology could offer new pathways for ZLD treatment of high salinity brines in a promising energy-efficient and economical manner.

7 Reference List

[1] B.K. Thakur, T. Chakraborty, Water Scarcity and Food Security: Implications for Developing Countries, in: 2020: pp. 1–9. doi:10.1007/978-3-319-69626-3_109-1.

[2] N. Hanasaki, S. Fujimori, T. Yamamoto, S. Yoshikawa, Y. Masaki, Y. Hijioka, M. Kainuma, Y. Kanamori, T. Masui, K. Takahashi, S. Kanae, A global water scarcity assessment under Shared Socio-economic Pathways - Part 2: Water availability and scarcity, Hydrol. Earth Syst. Sci. 17 (2013) 2393–2413. doi:10.5194/hess-17-2393-2013.

[3] J. Morrison, M. Morikawa, M. Murphy, P. Schulte, Water Scarcity & climate change, Water. 45 (2009) 1027–1039. doi:10.1007/s00267-010-9474-6.

[4] G. Ondrasek, Water scarcity and water stress in agriculture, in: Physiol. Mech. Adapt. Strateg. Plants Under Chang. Environ., 2014: pp. 75–96. doi:10.1007/978-1-4614-8591-9_4.

[5] R.B. Singh, D. Kumar, Water scarcity, in: Handb. Eng. Hydrol. Environ. Hydrol. Water Manag., 2014: pp. 519–544. doi:10.1201/b16766.

[6] L.S. Pereira, Water and Agriculture : Facing Water Scarcity and Environmental Challenges, J. Sci. Res. Dev. VII (2005) 1–26.

[7] N. Mancosu, R.L. Snyder, G. Kyriakakis, D. Spano, Water scarcity and future challenges for food production, Water (Switzerland). 7 (2015) 975–992. doi:10.3390/w7030975.

[8] V.G. Gude, Desalination and water reuse to address global water scarcity, Rev. Environ. Sci. Biotechnol. 16 (2017) 591–609. doi:10.1007/s11157-017-9449-7.

[9] A. Sood, V. Smakhtin, Can desalination and clean energy combined help to alleviate global water scarcity?, J. Am. Water Resour. Assoc. 50 (2014) 1111–

1123. doi:10.1111/jawr.12174.

[10] R. Hochstrat, T. Wintgens, C. Kazner, T. Melin, J. Gebel, Options for water scarcity and drought management—the role of desalination, Desalin. Water Treat. 18 (2010) 96–102. doi:10.5004/dwt.2010.1347.

[11] I. Bremere, M. Kennedy, A. Stikker, J. Schippers, How water scarcity will effect the growth in the desalination market in the coming 25 years, Desalination. 138 (2001) 7–15. doi:10.1016/S0011-9164(01)00239-9.

[12] H. March, D. Saurí, A.M. Rico-Amorós, The end of scarcity? Water desalination as the new cornucopia for Mediterranean Spain, J. Hydrol. 519 (2014) 2642–2651. doi:10.1016/j.jhydrol.2014.04.023.

[13] R. Kaplan, D. Mamrosh, H.H. Salih, S.A. Dastgheib, Assessment of desalination technologies for treatment of a highly saline brine from a potential CO2 storage site, Desalination. 404 (2017) 87–101. doi:10.1016/j.desal.2016.11.018.

[14] R. Semiat, Energy issues in desalination processes, Environ. Sci. Technol. 42 (2008) 8193–8201. doi:10.1021/es801330u.

[15] H. Thakkar, A. Sankhala, P. V Ramana, H. Panchal, A detailed review on solar desalination techniques, Int. J. Ambient Energy. (2018) 1–22. doi:10.1080/01430750.2018.1490351.

[16] T. Tong, M. Elimelech, The Global Rise of Zero Liquid Discharge for Wastewater Management: Drivers, Technologies, and Future Directions, Environ. Sci. Technol. 50 (2016) 6846–6855. doi:10.1021/acs.est.6b01000.

[17] H. Dahmardeh, H.A. Akhlaghi Amiri, S.M. Nowee, Evaluation of mechanical vapor recompression crystallization process for treatment of high salinity wastewater, Chem. Eng. Process. - Process Intensif. 145 (2019).

doi:10.1016/j.cep.2019.107682.

[18] Muhammad Yaqub, W. Lee, Zero-liquid discharge (ZLD) technology for resource recovery from wastewater: A review, Sci. Total Environ. 681 (2019) 551–563. doi:10.1016/j.scitotenv.2019.05.062.

[19] R. Bahar, M.N.A. Hawlader, L.S. Woei, Performance evaluation of a mechanical vapor compression desalination system, Desalination. 166 (2004) 123–127. doi:10.1016/j.desal.2004.06.066.

[20] D.D. Mara, Water, sanitation and hygiene for the health of developing nations, Public Health. 117 (2003) 452–456. doi:10.1016/S0033-3506(03)00143-4.

[21] United Nations General Assembly, International Decade for Action "Water for Life" 2005-2015. Focus Areas: The human right to water and sanitation, United Nations Resolut. 64/292. (2010).

[22] United Nations Water, Financing Universal Water, Sanitation and Hygiene under the Sustainable Development Goals., 2017. doi:10.1016/0002-9149(58)90231-5.

[23] United Nations, The Human Right to Water and Sanitation Milestones, Action. (2015) 1–4.

[24] Water And Sanitation Program Wsp, Poverty and Sanitation, Development. (2008) 32.

[25] United Nations, Un Water, Coping with Water Scarcity, Challenge of the 21st century, 2007. doi:10.3362/0262-8104.2005.038.

[26] Climate Change Contributes to Water Scarcity, in: Adapt. to a Chang. Clim. Arab Ctries., 2012: pp. 208–161. doi:10.1596/9780821394588_ch03.

[27] S.N. Gosling, N.W. Arnell, A global assessment of the impact of climate change

on water scarcity, Clim. Change. 134 (2016) 371–385. doi:10.1007/s10584-013-0853-x.

[28] Y. Jiang, China's water scarcity, J. Environ. Manage. 90 (2009) 3185–3196. doi:10.1016/j.jenvman.2009.04.016.

[29] A.C. Fuller, M.O. Harhay, Population growth, climate change and water scarcity in the Southwestern United States, Am. J. Environ. Sci. 6 (2010) 249–252. doi:10.3844/ajessp.2010.249.252.

[30] W.A. Abderrahman, T. Husain, Water scarcity, desalination and pollution, Ind. Environ. 27 (2004) 39–40.

[31] E. DeNicola, O.S. Aburizaiza, A. Siddique, H. Khwaja, D.O. Carpenter, Climate change and water scarcity: The case of Saudi Arabia, Ann. Glob. Heal. 81 (2015) 342–353. doi:10.1016/j.aogh.2015.08.005.

[32] M.M. Mekonnen, A.Y. Hoekstra, Sustainability: Four billion people facing severe water scarcity, Sci. Adv. 2 (2016) 1–7. doi:10.1126/sciadv.1500323.

[33] H. Sharon, K.S. Reddy, A review of solar energy driven desalination technologies, Renew. Sustain. Energy Rev. 41 (2015) 1080–1118. doi:10.1016/j.rser.2014.09.002.

[34] Living with Water Scarcity, Futur. Food J. Food, Agric. Soc. 2 (2015) 93–94.

[35] F.D. Owa, Water pollution: Sources, effects, control and management, Mediterr. J. Soc. Sci. 4 (2013) 65–68. doi:10.5901/mjss.2013.v4n8p65.

[36] P. Bhatt, A. Rani, Textile dyeing and printing industry: An environmental hazard, Asian Dye. 10 (2013) 51–54.

[37] R. Kant, Textile dyeing industry an environmental hazard, Nat. Sci. 04 (2012) 22–

26. doi:10.4236/ns.2012.41004.

[38] C. Parvathi, M.S.S. Parvin, Water pollution owing to water borne disease in {Coimbatore}, SELP J. Soc. Sci. VI (2015) 73–79.

[39] P. H., Water pollution and impact on child health, Indian J. Pract. Pediatr. 6 (2004) 219–223.

[40] E.R. Brown, E. Koch, T.F. Sinclair, R. Spitzer, O. Callaghan, J.J. Hazdra, Water pollution and diseases in fish (an epizootiologic survey), J. Environ. Pathol. Toxicol. 2 (1979) 917–925.

[41] R.P. Schwarzenbach, T. Egli, T.B. Hofstetter, U. von Gunten, B. Wehrli, Global Water Pollution and Human Health, Annu. Rev. Environ. Resour. 35 (2010) 109–136. doi:10.1146/annurev-environ-100809-125342.

[42] P.J. Landrigan, R. Fuller, S. Fisher, W.A. Suk, P. Sly, T.C. Chiles, S. Bose-O'Reilly, Pollution and children's health, Sci. Total Environ. 650 (2019) 2389–2394. doi:10.1016/j.scitotenv.2018.09.375.

[43] N.J. Ashbolt, Microbial contamination of drinking water and disease outcomes in developing regions, in: Toxicology, 2004: pp. 229–238. doi:10.1016/j.tox.2004.01.030.

[44] N.K. Dulvy, Y. Sadovy, J.D. Reynolds, Extinction vulnerability in marine populations, Fish Fish. 4 (2003) 25–64. doi:10.1046/j.1467-2979.2003.00105.x.

[45] V.C. Chong, P.K.Y. Lee, C.M. Lau, Diversity, extinction risk and conservation of Malaysian fishes, J. Fish Biol. 76 (2010) 2009–2066. doi:10.1111/j.1095-8649.2010.02685.x.

[46] J. Morillo, J. Usero, D. Rosado, H. El Bakouri, A. Riaza, F.J. Bernaola,

Comparative study of brine management technologies for desalination plants, Desalination. 336 (2014) 32–49. doi:10.1016/j.desal.2013.12.038.

[47] J.M. Arnal, M. Sancho, I. Iborra, J.M. Gozálvez, A. Santafé, J. Lora, Concentration of brines from RO desalination plants by natural evaporation, Desalination. 182 (2005) 435–439. doi:10.1016/j.desal.2005.02.036.

[48] T. Younos, Environmental Issues Environmental Issues of Desalination, Univ. Counc. Water Resour. J. Contemp. Water Res. Educ. Issue. 132 (2005) 11–18.

[49] J.R. Ziolkowska, Is Desalination Affordable?—Regional Cost and Price Analysis, Water Resour. Manag. 29 (2015) 1385–1397. doi:10.1007/s11269-014-0901-y.

[50] A. Purnama, H.H. Al-Barwani, M. Al-Lawatia, Modeling dispersion of brine waste discharges from a coastal desalination plant, Desalination. 155 (2003) 41–47. doi:10.1016/S0011-9164(03)00237-6.

[51] L.J. Falkenberg, C.A. Styan, The use of simulated whole effluents in toxicity assessments: A review of case studies from reverse osmosis desalination plants, Desalination. 368 (2015) 3–9. doi:10.1016/j.desal.2015.01.014.

[52] J.R. Ziolkowska, R. Reyes, Prospects for Desalination in the United States-Experiences From California, Florida, and Texas, in: Compet. Water Resour. Exp. Manag. Approaches US Eur., 2017: pp. 298–316. doi:10.1016/B978-0-12-803237-4.00017-3.

[53] J.S. Chang, Understanding the role of ecological indicator use in assessing the effects of desalination plants, Desalination. 365 (2015) 416–433. doi:10.1016/j.desal.2015.03.013.

[54] A. Valipour, N. Hamnabard, K.S. Woo, Y.H. Ahn, Performance of high-rate constructed phytoremediation process with attached growth for domestic

wastewater treatment: Effect of high TDS and Cu, J. Environ. Manage. 145 (2014) 1–8. doi:10.1016/j.jenvman.2014.06.009.

[55] R.G. Maliva, T.M. Missimer, R. Fontaine, Injection Well Options for Sustainable Disposal of Desalination Concentrate, IDA J. Desalin. Water Reuse. 3 (2011) 17–23. doi:10.1179/ida.2011.3.3.17.

[56] A. Panagopoulos, K.J. Haralambous, M. Loizidou, Desalination brine disposal methods and treatment technologies - A review, Sci. Total Environ. 693 (2019). doi:10.1016/j.scitotenv.2019.07.351.

[57] A.N. Roychoudhury, J. Petersen, Geochemical evaluation of soils and groundwater affected by infiltrating effluent from evaporation ponds of a heavy mineral processing facility, West Coast, South Africa, J. Geochemical Explor. 144 (2014) 478–491. doi:10.1016/j.gexplo.2014.02.016.

[58] S. Panta, P. Lane, R. Doyle, M. Hardie, G. Haros, S. Shabala, Halophytes as a Possible Alternative to Desalination Plants, in: Halophytes Food Secur. Dry Lands, 2016: pp. 317–329. doi:10.1016/b978-0-12-801854-5.00019-4.

[59] N. Ahmad, R.E. Baddour, A review of sources, effects, disposal methods, and regulations of brine into marine environments, Ocean Coast. Manag. 87 (2014) 1–7. doi:10.1016/j.ocecoaman.2013.10.020.

[60] M. Abualtayef, H. Al-Najjar, Y. Mogheir, A.K. Seif, Numerical modeling of brine disposal from Gaza central seawater desalination plant, Arab. J. Geosci. 9 (2016). doi:10.1007/s12517-016-2591-7.

[61] Regulating Effluents From India's Textile Sector New Commands and Compliance Monitoring for Zero Liquid Discharge, Law. 13 (2017) 13–31.

[62] S.Y. Alnouri, P. Linke, M.M. El-Halwagi, Accounting for central and distributed

zero liquid discharge options in interplant water network design, J. Clean. Prod. 171 (2018) 644–661. doi:10.1016/j.jclepro.2017.09.236.

[63] D.J. Barrington, G. Ho, Towards zero liquid discharge: The use of water auditing to identify water conservation measures, J. Clean. Prod. 66 (2014) 571–576. doi:10.1016/j.jclepro.2013.11.065.

[64] S. Ahirrao, Zero Liquid Discharge Solutions, in: Ind. Wastewater Treat. Recycl. Reuse, 2014: pp. 489–520. doi:10.1016/B978-0-08-099968-5.00013-1.

[65] C.W. Risk, Zero Liquid Discharge – A Real Solution?, China Water Risk. (2012).

[66] A.K. Popuri, P. Guttikonda, Zero liquid discharge (ZLD) industrial wastewater treatment system, Int. J. ChemTech Res. 9 (2016) 80–86.

[67] D.L. Shaffer, L.H. Arias Chavez, M. Ben-Sasson, S. Romero-Vargas Castrillón, N.Y. Yip, M. Elimelech, Desalination and reuse of high-salinity shale gas produced water: Drivers, technologies, and future directions, Environ. Sci. Technol. 47 (2013) 9569–9583. doi:10.1021/es401966e.

[68] M. Mickley, Survey of High-Recovery and Zero Liquid Discharge Technologies for Water Utilities, 2008. doi:10.1016/S0958-2118(08)70018-1.

[69] J. Bostjancic, R. Ludlum, Getting to Zero Discharge: How to Recycle That Last Bit of Really Bad Wastewater, GE. (2013).

[70] R.L. McGinnis, N.T. Hancock, M.S. Nowosielski-Slepowron, G.D. McGurgan, Pilot demonstration of the NH3/CO2 forward osmosis desalination process on high salinity brines, Desalination. 312 (2013) 67–74. doi:10.1016/j.desal.2012.11.032.

[71] T. Fukuzuka, K. Shimogori, H. Satoh, F. Kamikubo, Corrosion problems and their preventions of MSF desalination plant constructed with titanium tube,

Desalination. 31 (1979) 389–398. doi:10.1016/S0011-9164(00)88540-9.

[72] A. Panagopoulos, M. Loizidou, K.-J. Haralambous, Stainless Steel in Thermal Desalination and Brine Treatment: Current Status and Prospects, Met. Mater. Int. (2019). doi:10.1007/s12540-019-00398-w.

[73] M. Ahmed, W.H. Shayya, D. Hoey, A. Mahendran, R. Morris, J. Al-Handaly, Use of evaporation ponds for brine disposal in desalination plants, Desalination. 130 (2000) 155–168. doi:10.1016/S0011-9164(00)00083-7.

[74] A. Abdulsalam, A. Idris, T.A. Mohamed, A. Ahsan, An integrated technique using solar and evaporation ponds for effective brine disposal management, Int. J. Sustain. Energy. 36 (2017) 914–925. doi:10.1080/14786451.2015.1135923.

[75] B.D. Stanford, J.F. Leising, R.G. Bond, S.A. Snyder, Chapter 11 Inland Desalination: Current Practices, Environmental Implications, and Case Studies in Las Vegas, NV, Elsevier, 2010. doi:10.1016/S1871-2711(09)00211-6.

[76] K.K. Tanji, M.J. Herbel, Salt deposits in evaporation ponds : an environmental hazard ?, Calif. Agric. 46 (1992) 1–4.

[77] A. Giwa, V. Dufour, F. Al Marzooqi, M. Al Kaabi, S.W. Hasan, Brine management methods: Recent innovations and current status, Desalination. 407 (2017) 1–23. doi:10.1016/j.desal.2016.12.008.

[78] J.H. Tsai, F. Macedonio, E. Drioli, L. Giorno, C.Y. Chou, F.C. Hu, C.L. Li, C.J. Chuang, K.L. Tung, Membrane-based zero liquid discharge: Myth or reality?, J. Taiwan Inst. Chem. Eng. 80 (2017) 192–202. doi:10.1016/j.jtice.2017.06.050.

[79] K. Tanji, S. Ford, A. Toto, J. Summers, L. Willardson, Evaporation ponds: what are they; why some concerns, in: Manag. Irrig. Drain. Syst. Integr. Perspect., 1993: pp. 573–579.

[80] C. Fritzmann, J. Löwenberg, T. Wintgens, T. Melin, State-of-the-art of reverse osmosis desalination, Desalination. 216 (2007) 1–76. doi:10.1016/j.desal.2006.12.009.

[81] M. Elimelech, W.A. Phillip, The future of seawater desalination: Energy, technology, and the environment, Science (80-.). 333 (2011) 712–717. doi:10.1126/science.1200488.

[82] P. Bond, S. Veerapaneni, Zeroing in on ZLD technologies for inland desalination, J. / Am. Water Work. Assoc. 100 (2008). doi:10.1002/j.1551-8833.2008.tb09722.x.

[83] R. Bond, V. Veerapaneni, Reducing the costs for desalination with zero liquid discharge, in: Am. Water Work. Assoc. - Water Qual. Technol. Conf. Expo. 2007 Fast Tracks to Water Qual., 2007: pp. 1382–1392.

[84] A.F. Ismail, K.C. Khulbe, T. Matsuura, RO Membrane Fouling, in: Reverse Osmosis, 2019: pp. 189–220. doi:10.1016/b978-0-12-811468-1.00008-6.

[85] E.M.V. Hoek, J. Allred, T. Knoell, B.H. Jeong, Modeling the effects of fouling on full-scale reverse osmosis processes, J. Memb. Sci. 314 (2008) 33–49. doi:10.1016/j.memsci.2008.01.025.

[86] N. Penña, S. Gallego, F. del Vigo, S.P. Chesters, Evaluating impact of fouling on reverse osmosis membranes performance, Desalin. Water Treat. 51 (2013) 958–968. doi:10.1080/19443994.2012.699509.

[87] S. Jiang, Y. Li, B.P. Ladewig, A review of reverse osmosis membrane fouling and control strategies, Sci. Total Environ. 595 (2017) 567–583. doi:10.1016/j.scitotenv.2017.03.235.

[88] M.M. Damtie, R.H. Hailemariam, Y.C. Woo, K.D. Park, J.S. Choi, Membrane-

based technologies for zero liquid discharge and fluoride removal from industrial wastewater, Chemosphere. 236 (2019). doi:10.1016/j.chemosphere.2019.07.019.

[89] R. Bond, C. Owen, R. Teegarden, K. Browning, T.A. Davis, V. Veerapaneni, Zero liquid discharge desalination using a new electrodialysis technology, in: Water Qual. Technol. Conf. Expo. 2010, 2010: pp. 2412–2423.

[90] R. Bond, V. Veerapaneni, Zero liquid discharge desalination of brackish water with an innovative form of electrodialysis: Electrodialysis metathesis, Am. Water Work. Assoc. Annu. Conf. Expo. 2011, ACE 2011. (2011) 4289–4317.

[91] H.F. Xiao, D.D. Shao, Z.L. Wu, W.B. Peng, A. Akram, Z.Y. Wang, L.J. Zheng, W. Xing, S.P. Sun, Zero liquid discharge hybrid membrane process for separation and recovery of ions with equivalent and similar molecular weights, Desalination. 482 (2020). doi:10.1016/j.desal.2020.114387.

[92] S. Al Obaidani, M. Al-Abri, N. Al-Rawahi, Achieving the zero-liquid-discharge target using the integrated membrane system for seawater desalination, in: Recent Prog. Desalination, Environ. Mar. Outfall Syst., 2015: pp. 53–72. doi:10.1007/978-3-319-19123-2_5.

[93] S. Al Obaidani, E. Curcio, G. Di Profio, E. Drioli, The role of membrane distillation/crystallization technologies in the integrated membrane system for seawater desalination, Desalin. Water Treat. 10 (2009) 210–219. doi:10.5004/dwt.2009.923.

[94] A. Pérez-González, A.M. Urtiaga, R. Ibáñez, I. Ortiz, State of the art and review on the treatment technologies of water reverse osmosis concentrates, Water Res. 46 (2012) 267–283. doi:10.1016/j.watres.2011.10.046.

[95] A. Subramani, J.G. Jacangelo, Treatment technologies for reverse osmosis concentrate volume minimization: A review, Sep. Purif. Technol. 122 (2014) 472–

489. doi:10.1016/j.seppur.2013.12.004.

[96] R. Schwantes, K. Chavan, D. Winter, C. Felsmann, J. Pfafferott, Techno-economic comparison of membrane distillation and MVC in a zero liquid discharge application, Desalination. 428 (2018) 50–68. doi:10.1016/j.desal.2017.11.026.

[97] K. Loganathan, P. Chelme-Ayala, M. Gamal El-Din, Treatment of basal water using a hybrid electrodialysis reversal-reverse osmosis system combined with a low-temperature crystallizer for near-zero liquid discharge, Desalination. 363 (2015) 92–98. doi:10.1016/j.desal.2015.01.020.

[98] K. Loganathan, P. Chelme-Ayala, M. Gamal El-Din, Pilot-scale study on the treatment of basal aquifer water using ultrafiltration, reverse osmosis and evaporation/crystallization to achieve zero-liquid discharge, J. Environ. Manage. 165 (2016) 213–223. doi:10.1016/j.jenvman.2015.09.019.

[99] K.J. Lu, Z.L. Cheng, J. Chang, L. Luo, T.S. Chung, Design of zero liquid discharge desalination (ZLDD) systems consisting of freeze desalination, membrane distillation, and crystallization powered by green energies, Desalination. 458 (2019) 66–75. doi:10.1016/j.desal.2019.02.001.

[100] H. Guo, H.M. Ali, A. Hassanzadeh, Simulation study of flat-sheet air gap membrane distillation modules coupled with an evaporative crystallizer for zero liquid discharge water desalination, Appl. Therm. Eng. 108 (2016) 486–501. doi:10.1016/j.applthermaleng.2016.07.131.

[101] G. Chen, Y. Lu, W.B. Krantz, R. Wang, A.G. Fane, Optimization of operating conditions for a continuous membrane distillation crystallization process with zero salty water discharge, J. Memb. Sci. 450 (2014) 1–11. doi:10.1016/j.memsci.2013.08.034.

[102] Y. Oren, E. Korngold, N. Daltrophe, R. Messalem, Y. Volkman, L. Aronov, M.

Weismann, N. Bouriakov, P. Glueckstern, J. Gilron, Pilot studies on high recovery BWRO-EDR for near zero liquid discharge approach, Desalination. 261 (2010) 321–330. doi:10.1016/j.desal.2010.06.010.

[103] F. Macedonio, L. Katzir, N. Geisma, S. Simone, E. Drioli, J. Gilron, Wind-Aided Intensified eVaporation (WAIV) and Membrane Crystallizer (MCr) integrated brackish water desalination process: Advantages and drawbacks, Desalination. 273 (2011) 127–135. doi:10.1016/j.desal.2010.12.002.

[104] B. Murray, D. Mcminn, J. Gilron, WAIV TECHNOLOGY : AN ALTERNATIVE SOLUTION FOR BRINE MANAGEMENT, Water - J. Aust. Water Assoc. 42 (2015) 77.

[105] K.H. Mistry, M.A. Antar, J.H. Lienhard V, An improved model for multiple effect distillation, Desalin. Water Treat. 51 (2013) 807–821. doi:10.1080/19443994.2012.703383.

[106] C. Sharqawy, J.H. Lienhard V, S.M. Zubair, M.H. Sharqawy, The thermophysical properties of seawater: A review of existing correlations and data "The thermophysical properties of seawater: A review of existing correlations and data Terms of Use Creative Commons Attribution-Noncommercial-Share Alike 3.0 Therm, Desalin. Water Treat. 16 (2010) 354–380. doi:10.5004/dwt.2010.1079.

[107] K.G. Nayar, M.H. Sharqawy, L.D. Banchik, J.H. Lienhard, Thermophysical properties of seawater: A review and new correlations that include pressure dependence, Desalination. 390 (2016) 1–24. doi:10.1016/j.desal.2016.02.024.

[108] W. Wagner, A. Pruß, The IAPWS formulation 1995 for the thermodynamic properties of ordinary water substance for general and scientific use, J. Phys. Chem. Ref. Data. 31 (2002) 387–535. doi:10.1063/1.1461829.

A Copyright documentation

All images in the Introduction Section have been used in this thesis after obtaining official permissions from the respective journals. The licenses for reuse are provided by Elsevier and Copyright Clearance Center. All copyrighted images have been provided with appropriate citations to credit the respective journals and authors. Please see below for full citation and attribution information.

Figure 1.1, Figure 1.2: Muhammad Yaqub, W. Lee, Zero-liquid discharge (ZLD) technology for resource recovery from wastewater: A review, Sci. Total Environ. 681 (2019) 551–563. Downloaded from:(https://doi.org/10.1016/j.scitotenv.2019.05.062.) Accessed March 2020. Permission purchase order number: 4798300395247.

Figure 1.3, Figure 1.4: J.H. Tsai, F. Macedonio, E. Drioli, L. Giorno, C.Y. Chou, F.C. Hu, C.L. Li, C.J. Chuang, K.L. Tung, Membrane-based zero liquid discharge: Myth or reality?, J. Taiwan Inst. Cehm. Eng. 80(2017) 192-202. Downloaded from: (https://doi.org/10.1016/j.jtice.2017.06.050.) Accessed March 2020. Permission order number: 4799040411716.